THE ASTROPHYSICAL JOURNAL, 235:199–215, 1980 January 1

GRAVITATIONAL COLLAPSE TO NEUTRON STARS AND BLACK HOLES: COMPUTER GENERATION OF SPHERICAL SPACETIMES

STUART L. SHAPIRO[1]
Department of Astronomy and Center for Radiophysics and Space Research, Cornell University

AND

SAUL A. TEUKOLSKY[1]
Department of Physics and Center for Radiophysics and Space Research, Cornell University
Received 1979 April 23; accepted 1979 July 17

ABSTRACT

A new, general relativistic, hydrodynamical computer code for spherical, stellar collapse to neutron stars and black holes is presented. The code is employed to construct spacetimes for the geometrodynamical evolution of spherical masses which are initially at rest and obey an adiabatic Γ-law equation of state. Collapse to a black hole can be followed accurately; the evolution outside the event horizon can be determined far into the future without having the integration terminate because of spacetime singularities inside.

We use the code to address several fundamental points of principle regarding spherical, gravitational collapse and requiring a reliable, fully relativistic, numerical computation. We sample a variety of possible collapse scenarios, characterized by different masses, mass distributions, and equations of state, to examine stellar core collapse and its end fate. We distinguish three possible outcomes for adiabatic core collapse: homologous core bounce, nonhomologous core bounce, and catastrophic collapse to a black hole. Even a very massive stellar core may undergo a nonhomologous bounce and only later collapse to a black hole on a secular time scale rather than a dynamical one. Accretion-driven neutron star collapse is also treated numerically. The implications of our findings for realistic core collapse believed to occur in nature are considered.

Subject headings: black holes — hydrodynamics — relativity — stars: collapsed — stars: neutron

I. INTRODUCTION

We report in this paper the successful completion of a general relativistic, hydrodynamical computer code for spherical, stellar core collapse to neutron stars and black holes. We raise, and employ the code to partially answer, several questions of current astrophysical interest regarding core collapse and its end fate. We focus on issues which can only be answered by a reliable, fully relativistic, numerical calculation.

a) The Code

The computer code, particularly the hydrodynamics, is based on a code developed by Smarr and Wilson (see Wilson 1979*a*). A different approach to calculating the spacetime metric enables us to treat collapse to a black hole with reasonable numerical accuracy. Details of the computer code and its operation, together with all equations in differential and finite-difference form, will be presented elsewhere (Shapiro *et al.* 1980, hereafter SSTW). Suffice it to say that the code numerically solves the full set of Einstein equations for the time-dependent motion of a spherical distribution of matter immersed in an exterior vacuum. The matter is assumed to be at rest initially and to obey an adiabatic equation of state. The generalization to nonadiabatic behavior (e.g., via neutrino dissipation) is straightforward in principle, but has not yet been incorporated.

Our numerical scheme is characterized by several key features. We employ maximal time slicing to "hold back" the evolution (i.e., the advance of proper time) and the eventual formation of physically real singularities at the stellar center in the case of black hole formation (see Smarr and York 1978*b* and references therein). This allows us to follow the evolution in the outer (causally disconnected) stellar envelope. Relativistic configurations can be followed for *many* collapse time scales $\Delta t \gg GM/c^3$ *after* the initial appearance of an event horizon. The ability of the code to follow collapse after the formation of an event horizon represents, we feel, a significant advance over the pioneering scheme of May and White (1966, 1967). Bicknell and Henriksen (1979) have developed an alternate scheme using the method of characteristics which handles collapse successfully in the absence of shocks.

[1] Alfred P. Sloan Foundation Research Fellow.

The gravitational field is not dynamical in the case of spherical symmetry, and we use a form of Einstein's equations where the metric variables are determined anew at each instant of time by solving elliptic equations. This procedure, adopted after considerable experimentation, eliminates the direct propagation with time of numerical errors in the metric and ensures that the field quantities correspond to the matter distribution computed for each time slice to arbitrary high accuracy.

The fluid equations are differenced in Eulerian form, but the introduction of an arbitrary grid velocity, which moves with the matter near the stellar center, gives the code a mixed Euler-Lagrange character. The grid velocity, first introduced by Wilson, continuously relocates the radial grid markers so as to ensure "good grid coverage" of the bulk of the matter as the collapse progresses.

The basis for our confidence in the results reported below rests on the fact that our code has successfully passed a series of "reliability" tests. These included:

1) The numerical reproduction of the exact (Bondi-Tolman) solutions of spherical, dust collapse in both the relativistic and Newtonian domains.

2) Self-consistency between the computed exterior metric coefficients as measured by their ability to satisfy exact analytic relations for the Schwarzschild exterior solution. Since our outer boundary remains fixed and outside the star, unlike in a Lagrangian code, this agreement is nontrivial.

3) The ability to maintain highly relativistic, stable solutions of the Oppenheimer-Volkoff (OV) equation (see, e.g., Misner, Thorne, and Wheeler 1973 [MTW]) in hydrostatic equilibrium over many dynamical time scales.

4) The satisfactory handling of strong shocks, i.e., agreement with the relativistic Rankine-Hugoniot jump conditions for the (discontinuous) matter variables and the smooth variation of the (continuous) field variables across all shock fronts.

5) The monotonic growth of the (areal) radius of the event horizon, $r_A(H)$, during black hole formation and its asymptotic approach to the value $r_A(H) \to 2M$ as the time approaches infinity. Here $r_A(H)$ is defined to be $(A_H/4\pi)^{1/2}$, where A_H is the proper area of the event horizon, and M is the mass of the star.

These tests and others are elaborated in SSTW. We believe that the numerical code presented here may be the only one currently in existence which can pass all of these stringent tests.

b) Some Astrophysical Applications

We employ our computer code to address in a very preliminary and idealized fashion some of the long-standing, unanswered, theoretical questions regarding the geometrodynamics of stellar core collapse. These questions are:

1. What is the *minimum* mass of a black hole formed via the adiabatic collapse of a spherical stellar core of mass M? In particular, can the effective mass-energy "potential barrier" associated with equilibrium configurations (Harrison *et al.* 1965) be penetrated by low-mass cores with substantial inward, radial kinetic energy? Equivalently, does the inequality $M < M_{\max}$, where $M_{\max}$ is the maximum equilibrium mass associated with a particular cold equation of state, ensure that the collapsing configuration will eventually form a stable neutron star, or can it significantly overshoot its equilibrium density and form a black hole? Does the answer depend on the initial core profile and/or on the assumed equation of state?

2. How does collapse proceed to a black hole when $M > M_{\max}$? For example, it is widely believed that for sufficiently large masses, collapse invariably proceeds on a *dynamical* time scale. Is this view correct, or can the star bounce and oscillate for a while and/or significantly heat up via shock dissipation following its initial infall? What about mass blow-off?

3. What is the dynamical scenario by which the additional accretion of matter induces gravitational instability in a neutron star and leads to catastrophic collapse?

Several of these questions have been raised recently by other investigators, including Van Riper (1978, 1979) and Van Riper and Arnett (1978), who employed a general relativistic code similar to May and White (1966, 1967) to analyze spherical, adiabatic collapse. We feel, nevertheless, that a reexploration of these issues is useful for several reasons. The astrophysical importance of core collapse (e.g., for understanding spherical supernova explosions, estimating gravitational wave generation and neutrino emission during more realistic collapse scenarios, etc.), together with the numerous technical difficulties confronting all numerical treatments, warrant another independent analysis. Moreover, the motivation for using an *adiabatic* code to analyze collapse has been strengthened by the recent realization of the importance of neutrino trapping (Arnett 1977; Saenz and Shapiro 1979; Wilson 1979*a*). In addition, the present investigation can follow collapse to black holes well after the initial appearances of event horizons and trapped surfaces. Infinite densities leading to physical and numerical singularities do not occur in finite (coordinate) time as in May and White. Finally, the Eulerian grid employed here, in contrast to the comoving, Lagrangian grid of May and White, does not lead to discontinuities in the metric across shocks (Smarr, Taubes, and Wilson 1979), which would pose problems in deciphering the spacetime geometry numerically.

By following numerous adiabatic collapse sequences involving cores initially at rest, pressure deficient, and obeying an isentropic Γ-law equation of state, we find that barrier penetration and black hole formation do not occur whenever $M < M_{\max}$. We find that for all Γ in the range $4/3 < \Gamma \leq 2$ and $M < M_{\max}$, collapse leads to a hydrodynamical bounce and reflection shock followed either by quasi-homologous oscillations of the "inner core" (cf. Van Riper 1978), or by the nonhomologous, quasi-static settling of the shock-heated matter into a new (high entropy) equilibrium state. Such nonhomologous behavior occurs whenever the initial pressure deficiency is sufficiently great that the infall can proceed on free-fall time scales ($\propto \rho^{-1/2}$) and the very dense, central regions collapse faster and bounce sooner than the overlying layers. For the same reason, nonhomologous collapse and shock-induced, high-entropy equilibrium results *even when* $M > M_{\text{max}}$, provided $\Gamma > 4/3$ and the initial pressure deficiency and core radius are large. In these cases, the final (inevitable) collapse to a black hole must await the dissipation of the shock-induced thermal energy, which presumably occurs on slow, *secular* (neutrino dissipation) time scales. The implications of these results for realistic core collapse are explored below.

c) *Format*

In § II we present the key definitions and basic partial differential equations which were employed to evolve the matter and field quantities in our computations. We also state the boundary conditions and initial conditions necessary to specify a space time. In § III, we describe some astrophysical applications of the computer code to problems involving stellar core collapse and accretion-driven, neutron star collapse. In § IV we use our numerical results to discuss the geometry of spherical collapse. Here we discuss the implications of our choices of the maximal slicing gauge condition and isotropic ("minimum shear") coordinates. We also examine the growth of event horizons during black hole formation. Finally, in § V, we briefly summarize some limitations of our current code and describe our future plans for removing these limitations by generalizing the code to handle more realistic collapse behavior.

II. BASIC EQUATIONS

We list here, without derivation, the equations in the form we solve them. Full details are given in SSTW.

The metric is written in isotropic form,

$$ds^2 = -(\alpha^2 - A^2\beta^2)dt^2 + 2A^2\beta dr dt + A^2(dr^2 + r^2 d\theta^2 + r^2 \sin^2\theta d\phi^2) . \tag{1}$$

Here α and β are the lapse and shift functions of Arnowitt, Deser, and Misner (1962); see also Smarr and York (1978*a*, *b*). We use units with $c = G = 1$.

The stress-energy tensor is that of a perfect fluid,

$$T_{\mu\nu} = [\rho_0(1 + \epsilon) + P]U_\mu U_\nu + P g_{\mu\nu} , \tag{2}$$

where ρ_0 is the proper rest-mass density, ϵ the specific internal energy density, P the pressure, and U_μ the fluid 4-velocity. Define the following variables:

$$U = \alpha U^t , \tag{3}$$

$$D = \rho_0 U , \tag{4}$$

$$E = \rho_0 \epsilon U , \tag{5}$$

$$S_\mu = [\rho_0(1 + \epsilon) + P]UU_\mu , \tag{6}$$

$$v = U^r/U^t , \tag{7}$$

$$\gamma^{1/2} = A^3 r^2 . \tag{8}$$

Note that D ("rest-mass density"), E ("energy density"), and S_μ ("momentum density") are α times the corresponding quantities defined by Wilson (1972, 1979*a*). The equation of particle conservation, $(\rho_0 U^\mu)_{;\mu} = 0$, and energy-momentum conservation, $T^{\mu\nu}{}_{;\nu} = 0$, yield the following equations for the time evolution of D, E, and S_r:

$$\partial_t D = -\gamma^{-1/2}[\partial_r(D\gamma^{1/2}v) + D\partial_t\gamma^{1/2}] , \tag{9}$$

$$\partial_t S_r = -\gamma^{-1/2}[\partial_r(S_r\gamma^{1/2}v) + S_r\partial_t\gamma^{1/2}] - \alpha\partial_r P - \alpha S^t\partial_r\alpha + S_r\partial_r\beta - \tfrac{1}{2}(S_r{}^2/S^t)\partial_r(A^{-2}) , \tag{10}$$

$$\partial_t E = -\gamma^{-1/2}[\partial_r(E\gamma^{1/2}v) + E\partial_t\gamma^{1/2} + P\partial_t(U\gamma^{1/2}) + P\partial_r(U\gamma^{1/2}v)] . \tag{11}$$

The 4-velocity normalization condition, $U^\mu U_\mu = -1$, together with equation (6), gives an algebraic condition for S^t:

$$S^t = [(D + E + PU)^2 + S_r{}^2/A^2]^{1/2}/\alpha , \tag{12}$$

and so U and v can be found from

$$U = \alpha S^t/(D + E + PU) \, , \tag{13}$$

$$v = S_r/(A^2 S^t) - \beta \, . \tag{14}$$

For a general equation of state,

$$P = P(\rho_0, \epsilon) \, , \tag{15}$$

equations (12) and (13) have to be solved iteratively for S^t and U. For the special case of a Γ-law equation of state, $P = (\Gamma - 1)\rho_0\epsilon$, i.e.,

$$PU = (\Gamma - 1)E \, , \tag{16}$$

equation (12) becomes an explicit equation for S^t.

After evolving the hydrodynamic quantities D, E, and S_r forward in time, one needs to find the metric functions α, A, and β on the new time slice. To do this, we introduce the extrinsic curvature tensor K_{ij}. We impose the "maximal slicing" condition $K \equiv \text{Trace}\,(K_{ij}) = 0$, so that

$$K^r{}_r = -2K^\theta{}_\theta = -2K^\phi{}_\phi \, . \tag{17}$$

This condition, together with Einstein's field equations, determines α by

$$\partial_r(Ar^2\partial_r\alpha) = \alpha A^3 r^2[8\pi(D + E + PU)U(2 - 1/U^2) + 16\pi P + 3(K^r{}_r)^2]/2 \, . \tag{18}$$

The Hamiltonian and momentum constraint equations give A and $K^r{}_r$:

$$r^{-2}\partial_r(r^2\partial_r A^{1/2}) = -A^{5/2}[8\pi(D + E + PU)U - 8\pi P + 3(K^r{}_r)^2/4]/4 \, , \tag{19}$$

$$K^r{}_r = \frac{8\pi}{A^3r^3}\int_0^r A^3r^3S_r dr \, . \tag{20}$$

The definition of K_{ij} in terms of derivatives of the metric can be manipulated to give

$$\beta = -\tfrac{3}{2}r\int_r^\infty \alpha K^r{}_r dr/r \, . \tag{21}$$

The boundary conditions on α, β, and A as $r \to \infty$ are that α and A tend to unity, while $\beta \to 0$. In numerical work, however, one wishes to impose the boundary conditions at a finite value of r outside the star. One relation comes from matching the metric (1) outside the star to the static Schwarzschild metric in isotropic coordinates:

$$ds^2 = -\frac{[1 - M/(2\bar{r})]^2}{[1 + M/(2\bar{r})]^2}dt_s{}^2 + \left(1 + \frac{M}{2\bar{r}}\right)^4(d\bar{r}^2 + \bar{r}^2d\theta^2 + \bar{r}^2\sin^2\theta d\phi^2) \, . \tag{22}$$

Here $t_s = t_s(t, r)$ is the Schwarzschild time coordinate and $\bar{r} = \bar{r}(t, r)$ is the isotropic radial coordinate. The matching yields

$$1 + r(\partial_r A)/A = [1 - 2M/(Ar) + r^2A^2K^r{}_r{}^2/4]^{1/2} \tag{23}$$

(details in SSTW). Since $K^r{}_r \sim 1/r^3$ as $r \to \infty$ (cf. eq. [20]), the approximate solution of equation (23) is

$$A = \left(1 + \frac{M}{2r}\right)^2\left[1 + O\left(\frac{1}{r^4}\right)\right] , \tag{24}$$

which is adequate for numerical work.

The maximal slicing equation (18) can be solved analytically outside the star to give

$$\alpha = 1 + r(\partial_r A)/A + \text{const.}\,[1/r + O(1/r^2)] \, . \tag{25}$$

The constant is in principle determined by the boundary condition $\partial_r\alpha = 0$ at $r = 0$; in practice, we took the constant equal to zero and set the outer boundary at $r \gg M$.

The asymptotic solution of equation (21) gives

$$\beta = -\tfrac{1}{2}rK^r{}_r[1 + O(1/r)] \, . \tag{26}$$

The boundary conditions at the center of the star are that

$$0 = \partial_r\alpha = \partial_r A = \beta = K^r{}_r = \partial_r D = \partial_r E = S_r \, . \tag{27}$$

Shocks are handled by an empirical, relativistic generalization of the von Neumann artificial viscosity

$$q = \kappa D(\Delta v)^2/\alpha\,, \quad \Delta v < 0$$
$$= 0\,, \qquad \Delta v > 0\,, \tag{28}$$

which is added to the pressure in equations (10) and (11). Here $\Delta v = v_{i+1} - v_i$ is the velocity difference between neighboring grid points in the finite-difference scheme, and κ is a dimensionless number of order unity.

A typical computer run involves first setting up the initial matter profile. This is usually most conveniently done with a Schwarzschild radial coordinate. We then transform to isotropic coordinates. The matter variables are evolved to the next time slice via equations (9)–(11). We then determine the metric at the new time via equations (18)–(21). Care is needed in handling the nonlinearities in A in the Hamiltonian equation (19). We make a first guess for A at the new time from the evolution equation

$$\partial_t A = \beta(\partial_r A + A/r) + \tfrac{1}{2}\alpha A K^r{}_r\,, \tag{29}$$

and then refine this value of A by iterating equation (19). Essentially we are solving an initial-value problem for the metric at each time slice so that the metric corresponds to the matter distribution to sufficient accuracy. Direct solution of the evolution equation (29) is inherently inaccurate for collapse to a black hole as discussed in SSTW.

As the evolution proceeds, we track Lagrangian matter tracers r_i by integrating the equations

$$\frac{dr_i}{dt} = v(t, r_i)\,. \tag{30}$$

Similarly, we compute outgoing radial light-ray trajectories r_j from

$$\frac{dr_j}{dt} = \alpha(t, r_j)/A(t, r_j) - \beta(t, r_j)\,. \tag{31}$$

We also test for the existence of trapped surfaces, i.e., 2-spheres such that the outgoing radial light rays are converging. The condition for this is that

$$\frac{d}{dt}(4\pi A^2 r^2) \le 0\,, \tag{32}$$

where d/dt is the total time derivative taken along an outgoing radial light ray. The outermost trapped surface is called the apparent horizon; its location can be determined on any time slice by finding the largest radius at which equality holds in equation (32). This is equivalent to the relation

$$1 + r(\partial_r A)/A + ArK^r{}_r/2 = 0\,. \tag{33}$$

The true event horizon always lies outside the apparent horizon; in fact, the event horizon can form before any trapped surfaces do (Hawking and Ellis 1973). The event horizon can only be found by following light rays via equation (31) and seeing which escape to infinity and which are trapped by the black hole. For a stationary black hole, the apparent horizon and the event horizon coincide.

III. SOME ASTROPHYSICAL APPLICATIONS

a) *Stellar Core Collapse*

In this section we employ our numerical code to examine the hydrodynamics of core collapse to a neutron star or a black hole. We consider configurations which are initially static and isentropic, with an equation of state given by

$$P = K\rho_0{}^\Gamma\,, \quad K, \Gamma \text{ constant}\,. \tag{34}$$

During the subsequent dynamical evolution, the pressure is governed by equation (16).

By varying K and Γ, as well as the total mass and initial mass-energy density profile, we can follow and distinguish a variety of possible dynamical scenarios which can occur during spherical, adiabatic collapse. The principal aim of this paper is the study of such a broad sample of possible collapse scenarios, rather than the generation of a specific collapse model which claims to represent the "true" implosion of a "realistic" ($\sim 1.4\ M_\odot$) stellar core.

i) *Numerical Results*

To establish natural points of reference to evaluate subsequent dynamical calculations, we first construct sequences of *equilibrium* models by solving the OV equation (see, e.g., MTW 1973) employing the equation of

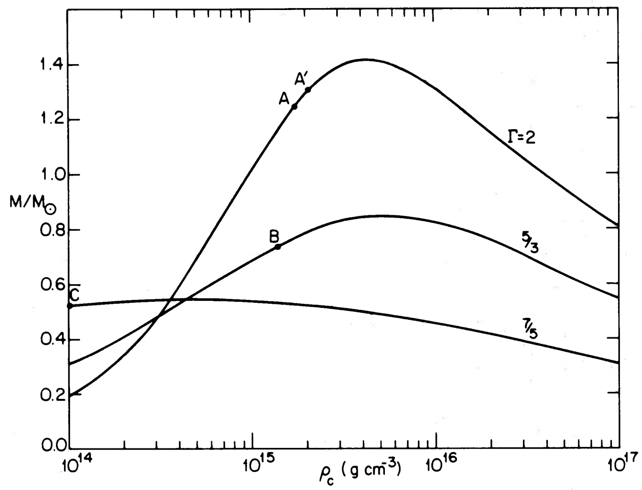

FIG. 1.—Equilibrium solutions of the OV equation are plotted for three different polytropic equations of state. Configurations labeled A, A', B, and C are described in Table 1 and used in numerical experiments as explained in the text.

state given by equation (34). Results are plotted in Figure 1 for three equilibrium sequences defined by $(\Gamma, K) = (2, 9.2 \times 10^4)$, $(5/3, 5.38 \times 10^9)$, and $(7/5, 3.5 \times 10^{13})$. Several key parameters for the specific equilibrium models labeled in the figure and for the maximum mass configurations are listed in Table 1. For $\Gamma = 5/3$, the adopted equation of state corresponds to ideal, cold, degenerate nonrelativistic neutrons. For $\Gamma = 2$ and $7/5$, the equation of state has been chosen to yield a pressure equal to the nonrelativistic Fermi neutron gas pressure at $\rho_0 = 2 \times 10^{14}$ g cm^{-3} (i.e., nuclear density), but becomes harder ($\Gamma = 2$) or softer ($\Gamma = 7/5$) at higher densities. Harder equations of state are associated with greater maximum masses and central redshift, as is evident from the values of M, R_s, and α_c in Table 1. Here R_s is the stellar radius in Schwarzschild coordinates. We recall that on a given equilibrium curve, models with central mass-energy densities less than the maximum mass central density satisfy $dM/d\rho_c > 0$ and are dynamically stable against adiabatic, radial oscillations; those models with higher densities are not stable (Harrison *et al.* 1965).

For each of the three adopted equations of state we have performed a variety of dynamical collapse calculations. Our "canonical" set of initial models for collapse consists of static configurations with mass-energy density profiles self-similar to an arbitrarily chosen stable model on the equilibrium curve; these models have mass M and radius R and a density profile in Schwarzschild coordinates given by $\rho(r) = (M/M_{\rm eq})\rho_{\rm eq}(r')$ where $r' = rR_{\rm eq}/R$. The selected equilibrium models for the $\Gamma = 2$, $5/3$, $7/5$ cases are denoted by A, B, and C, respectively, in Figure 1 and Table 1. All lie near, but slightly below, the corresponding maximum mass configuration. The initially static configurations are constructed with various masses and radii which, in general, satisfy $M \geq M_{\rm eq}$, $R \geq R_{\rm eq}$. By construction, these objects, which satisfy equation (34), are pressure (and entropy) deficient when released at $t = 0$ and immediately undergo gravitational collapse. They may be viewed as "former" equilibrium models which, when "puffed up" to large radii and low densities and in some cases endowed with greater total mass, must undergo collapse to return to the high-density domain characterizing their equilibrium progenitors. They model cold, isentropic stellar cores which are on the verge of collapse to a final neutron star or black hole state.

Representative collapse behavior is illustrated in Figure 2 for $\Gamma = 5/3$. Here we plot the spacetime world lines of Lagrangian matter tracers in the core for three qualitatively different collapse scenarios. Each world line is

TABLE 1

STABLE EQUILIBRIUM CONFIGURATIONS OBEYING $P = K\rho_0{}^\Gamma$

Γ	K[a] (cgs)	$M/M_\odot$	R_s/M	$\rho_{0,c} \times 8\pi M^2$	ρ_c (10^{15} g cm^{-3})	α_c	Comments
2......	9.2×10^4	1.42	4.18	0.264	4.32	0.434	maximum mass
		1.31	5.43	0.120	2.03	0.577	$M_{A'}$
		1.25	5.89	0.094	1.70	0.624	M_A
5/3....	5.38×10^9	0.844	6.72	0.126	5.38	0.600	maximum mass
		0.737	11.1	0.027	1.36	0.772	M_B
7/5....	3.5×10^{13}	0.545	32.1	0.0047	0.42	0.886	maximum mass
		0.526	51.4	0.0011	0.10	0.930	M_c

[a] For $\Gamma = 5/3$, $P \equiv P$ (degenerate, nonrelativistic neutrons); for all Γ, $P \equiv P(\Gamma = 5/3)$ at $\rho_0 = 2 \times 10^{14}$ g cm^{-3}.

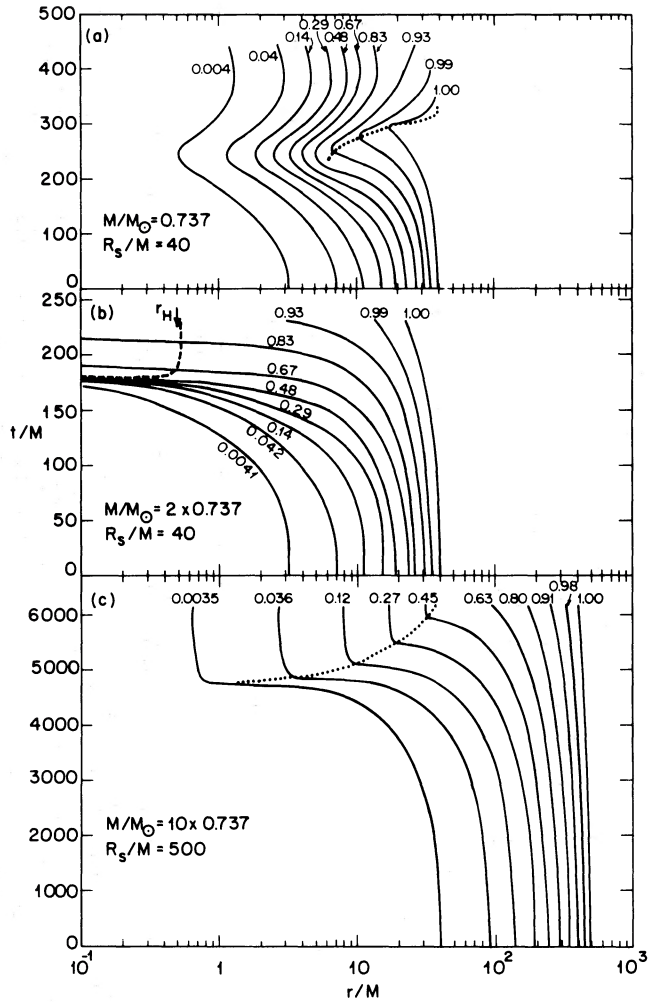

FIG. 2.—Spacetime diagrams of the world lines of Lagrangian matter tracers for the collapse of stars composed of ideal neutrons, initially degenerate and nonrelativistic. Each tracer is labeled by the fixed fraction of baryons interior to it. Dotted lines in (*a*) and (*c*) denote the shock front; the dashed line in (*b*) denotes the event horizon. Collapse leads to a homologous bounce in (*a*), formation of a black hole in (*b*), and a nonhomologous bounce in (*c*).

labeled by the (fixed) fraction of the total rest mass contained within the given Lagrangian radius during the collapse. Eulerian snapshots of the rest density profile $\rho_0(r)$ and the matter velocity profile, $v(r)$, are shown for different time slices for these three cases in Figures 3 and 4, respectively.

Figure 2 clearly exhibits our general finding that, depending on initial conditions, *spherical, adiabatic collapse with* $\Gamma > 4/3$ *leads either to* (*1*) *homologous core bounce, following maximum compression,* (*2*) *nonhomologous core bounce, or* (*3*) *catastrophic collapse to a black hole.* For moderate initial core radii $R \gtrsim R_{\mathrm{eq}}$ and pressure deficiencies, core collapse results in a homologous bounce whenever $M \lesssim M_{\max}$ and a black hole whenever $M \gtrsim M_{\max}$, as shown in Figures 2*a*, *b*. (Here the subscript "max" refers to the maximum mass configurations.) A general description of homologous bounce behavior following spherical, adiabatic core collapse has been presented previously by Van Riper (1978). Homologous bounce for the conditions considered here is accompanied by large-amplitude, adiabatic oscillations of the inner regions of the core at high central density ($\Delta\rho_c/\rho_c \gtrsim 10$), following the initial infall of the core to a point of maximum compression. Upon the initial rebound, the "inner core" drives a reflection shock through the infalling layers of the outer mantle, causing the "outer core" to undergo a velocity reversal which, in some cases, leads to the complete ejection of the outermost layers. The mass fraction separating the homologous inner core from the shock-accelerated outer core depends on initial conditions, the adopted equation of state, the assumed core parameters, etc. We shall henceforth characterize a bounce as homologous if the "inner core," as depicted above, contains at least 50% of the total rest mass, as in the example illustrated in Figures 2*a*, 3*a*, and 4*a*. (The choice of 50% is somewhat arbitrary.)

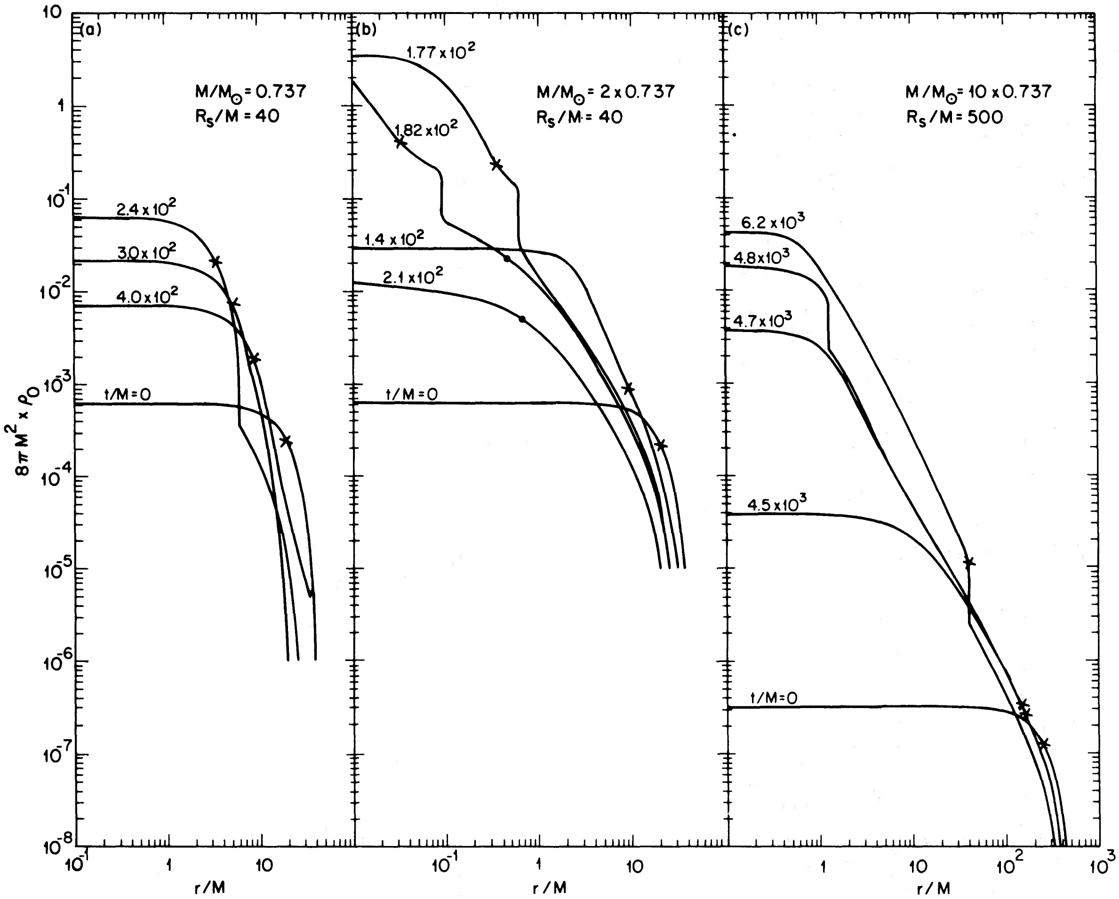

FIG. 3.—Eulerian snapshots at different times of the rest mass density profiles for the collapse cases shown in Fig. 2. Crosses label the radial coordinate enclosing 50% of the baryons. Dots in (*b*) denote the position of the event horizon. Sharp jumps in the density profiles result from the propagation of strong shocks.

For large initial core radii $R \gg R_{eq}$ and substantial pressure deficiencies, collapse leads to a nonhomologous bounce following maximum compression at high densities, *even when* $M > M_{max}$. This situation is illustrated in Figures 2*c*, 3*c*, and 4*c*. Here, the collapse proceeds on free-fall time scales, t_{ff}, as in the case of pressureless dust, until the collapse is finally halted by adiabatic pressure buildup at the center. Since t_{ff} varies as $\rho^{-1/2}$, the dense, central regions collapse faster and bounce first, and ultimately drive a reflection shock through a very large fraction of the infalling core. The shock-heated core material then accretes slowly onto the central regions. This gradual settling occurs along a high-temperature adiabat and results in a quasi-static equilibrium configuration corresponding to the new, shock-induced, high-entropy equation of state ($P > K\rho_0{}^\Gamma$). At the termination of our numerical integrations for the collapse of a cold, massive neutron core with $M/M_\odot = 10 \times 0.737$ (cf. $M_{max}/M_\odot = 0.844$) and $R_s/M = 500$ ($R_{s,max}/M = 6.72$) the pressure at the radius containing 50% of the rest mass has risen by a factor of 300 above the cold, degenerate value, due to shock-heating. The equation of state has become primarily that of a hot, thermal (Maxwell-Boltzmann) neutron gas throughout the bulk of the core and can easily support the massive configuration against further collapse. The temperature associated with the pressure and density at the half-mass radius has risen from an initial value of $T = 0$ to $T = 7.5 \times 10^{10}$ K and satisfies $kT/m_n \approx 0.3M/R$, reflecting an efficient conversion of gravitational potential energy to thermal energy by the shock, following collapse and bounce. Correspondingly, the entropy per baryon has risen from a value of 0 to $s/k = 9.9$, where k is Boltzmann's constant. Further collapse requires the dissipation of this shock-induced thermal energy, which can only occur on secular (e.g., neutrino dissipation) time scales, even when $M > M_{max}$. In striking contrast, homologous bounce results in no significant heating or thermal pressure and entropy generation in the large inner core, so it can only support the adiabatic oscillations of a mass $M < M_{max}$.

Nonhomologous bounce is thus distinguished from homologous bounce by (1) the formation of a shock near the very center of the rebounding core following maximum compression, and its subsequent outward propagation through the *bulk* of the infalling matter, (2) a substantial shock-induced entropy and temperature increase

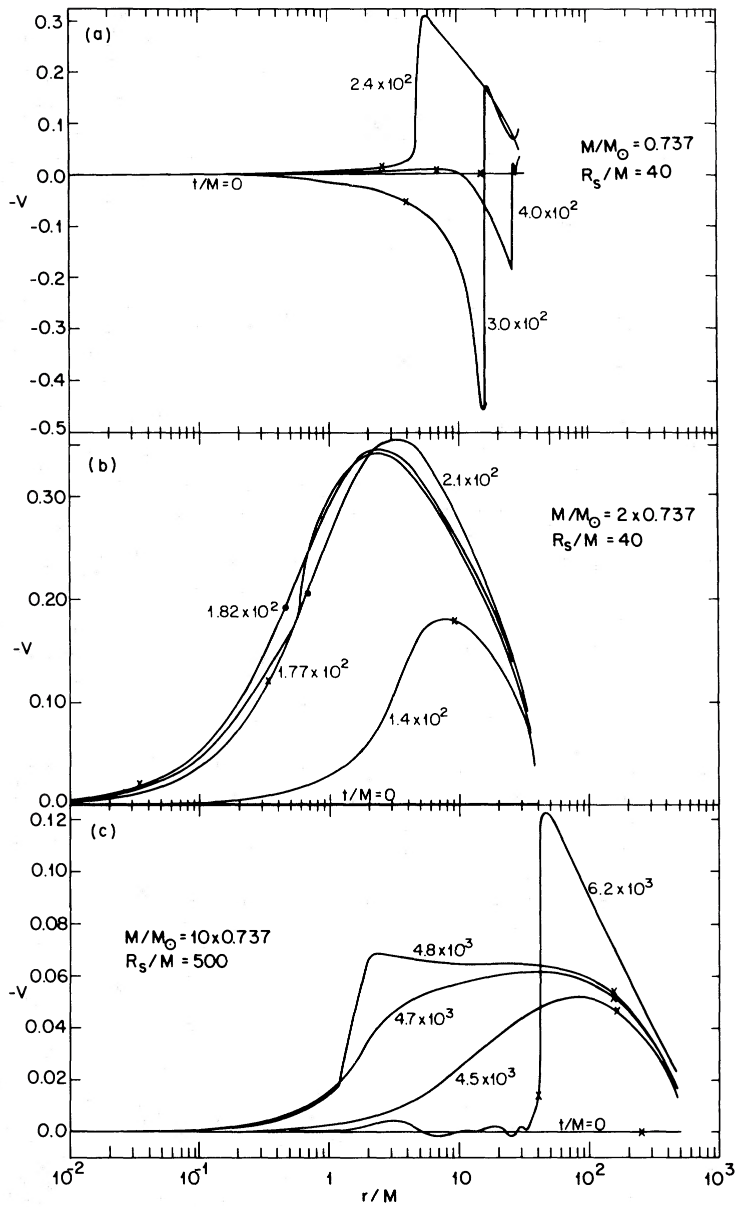

FIG. 4.—Eulerian shapshots at different times of the inward radial velocity for the collapse cases shown in Fig. 2

throughout most of the core, (3) the absence of large-amplitude, homologous oscillations following maximum compression, and (4) the formation of a hot, quasi-static equilibrium configuration appropriate for the new, high-entropy equation of state and stable against further collapse on dynamical time scales. A nonhomologous bounce can evidently postpone the inevitable collapse to a black hole of a configuration with $M > M_{\max}$ until the thermal pressure support is dissipated. Nonhomologous behavior will occur whenever Γ exceeds 4/3 and the pressure deficiency in the central regions of the collapsing configuration becomes sufficiently large that the infall speed exceeds the characteristic sound speed there, allowing the collapse to proceed nonuniformly on free-fall time scales. Of course, when $\Gamma < 4/3$, the collapse is nonhomologous, but no stable equilibrium solutions exist and collapse always leads directly to a black hole on a dynamical time scale.

When the initial core radius and pressure deficiency are not too large, but the mass exceeds $M_{\max}$, the collapse proceeds subsonically and quasi-homologously to a black hole, as shown in Figures 2*b*, 3*b*, and 4*b*. Spherical, adiabatic collapse to a black hole from rest is rather undramatic hydrodynamically: mass flows smoothly through the event horizon, which first appears at the stellar center and moves monotonically outward in area (see § IV);

TABLE 2

PARAMETERS FOR THE CANONICAL COLLAPSE SEQUENCE

		$t = 0$			$t = t_f$[b]					
Γ	M[a]	R_s/M	$\rho_{0,c} \times 8\pi M^2$	α_c	t_f/M	$\rho_{0,c} \times 8\pi M^2$	K_f/K[c]	α_c	$r_A(H)/M$	Outcome[d]
2.............	M_A	20	2.8 (−3)	0.897	1.1 (2)	0.24	1.1	0.44	...	bounce (h)
	$2M_A$	20	2.8 (−3)	0.897	87.	2.8	...	8.8 (−4)	1.6	black hole
	$2M_A$	40	3.5 (−4)	0.949	2.2 (2)	0.14	31.	0.73	...	bounce (nh)
	$10M_A$	40	3.5 (−4)	0.949	4.2 (2)	2.6	520.	0.63	...	bounce (nh)
5/3...........	M_B	20	4.9 (−3)	0.877	1.7 (2)	0.14	1.0	0.56	...	bounce (h)
	$2M_B$	20	5.0 (−3)	0.879	79.	2.4	...	2.2 (−2)	1.4	black hole
	M_B	40	6.3 (−4)	0.939	4.4 (2)	9.0 (−3)	1.0	0.86	...	bounce (h)
	$2M_B$	40	6.3 (−4)	0.940	2.3 (2)	6.1	...	3.1 (−16)	2.1	black hole
	$2M_B$	500	3.2 (−7)	0.995	6.6 (3)	2.9 (−3)	29.	0.95	...	bounce (nh)
	$10M_B$	500	3.2 (−7)	0.995	6.2 (3)	4.2 (−2)	297.	0.94	...	bounce (nh)
7/5...........	M_C	500	1.2 (−6)	0.993	1.1 (4)	9.7 (−5)	1.0	0.97	...	bounce (h)
	$2M_C$	500	1.2 (−6)	0.993	4.7 (3)	18.	...	1.6 (−6)	1.0	black hole
4/3...........	(M)[e]	500	4.8 (−8)	0.997	1.8 (4)	2.7	...	6.2 (−16)	2.3	black hole

[a] Profile of mass-energy density is self-similar to the stable equilibrium profile of mass $M_{(A,B,C)}$ for $\Gamma \equiv (2, 5/3, 7/5)$, respectively (see Table 1).

[b] $t = t_f$ is the time at the (arbitrary) termination of the numerical integrations.

[c] $K_f = (P/\rho_0{}^\Gamma)_f$ is evaluated near the radius containing $\frac{1}{2}$ of the total rest mass.

[d] h = homologous; nh = nonhomologous.

[e] For arbitrary mass with a homogeneous profile and $P = 0.5P_{\rm eq}$ initially.

the matter forms a high-density central spike whose growth with time is controlled by the maximal slicing condition. *No physical or numerical singularities arise during the computation* (cf. May and White 1966). As is evident in Figure 3*b*, a strong shock wave forms in the outer mantle of the collapsing core with $M/M_\odot = 2 \times 0.737$ and $R_s/M = 40$. However, the shock front is eventually swept into the event horizon by the infalling matter, thereby preventing its outward propagation through the outer layers of the core. Note that the velocity profile near the shock plotted in Figure 4*b* has been smoothed somewhat by plotting velocities in the static (rather than comoving) frame. The density at the center of the star increases monotonically, although this is not apparent on the logarithmic radial scale used in Figure 2*b*. A substantial fraction ($\gtrsim 90\%$) of the rest mass has passed within the event horizon in this example before we arbitrarily terminate our integrations. The geometry of this collapse case is explored in § IV.

Similar hydrodynamic behavior, leading to homologous and nonhomologous bounces and to the formation of black holes, occurs for the collapse sequences with $\Gamma = 2$ and 7/5. The results for all the numerical integrations are summarized in Table 2, where the initial and final core parameters are compared for representative runs. The time evolution of the central mass-energy density $\rho_{0,c}$ is shown in Figure 5 for these cases. The initially static configurations with harder equations of state which we considered suffered greater pressure deficiency than configurations with softer equations at comparable radii. Consequently, for cores with harder equations of state, nonhomologous bounces resulted from collapse from smaller initial radii. In fact, for $\Gamma = 2$, nonhomologous bounce occurred in all cases for $R_s/M \geq 40$ and prevented the catastrophic collapse to black holes of cores with total masses roughly 10 times the maximum mass for the same equation of state. For $\Gamma = 7/5$, however, nonhomologous bounce did not occur even for $R_s/M = 500$, and the configurations either bounced homologously or collapsed to black holes depending on whether M was less than or greater than $M_{\max}$. As expected, catastrophic collapse always occurred for a pressure-deficient configuration with $\Gamma = 4/3$, as demonstrated by the last entry in Table 2.

From our numerical experiments we find that spherical, adiabatic collapse from rest of a (pressure deficient) isentropic core with $M < M_{\max}$ never results in a black hole; i.e., *mass-energy "barrier penetration" does not occur* in such cases. Similar results have been found by Van Riper and Arnett (1978) and Van Riper (1979). We have already emphasized the related fact that, *in many cases with $M > M_{\max}$, collapse to a black hole does not occur on a dynamical time scale*, because of shock heating following a nonhomologous bounce. Finally, in all cases we have examined, *collapse from rest which does lead to a black hole does not result in any mass ejection.* Some mass ejection can occur for homologous bounces but none occurs for nonhomologous bounces (cf. Fig. 2).

ii) *Astrophysical Implications*

The hydrodynamical calculations described above are of great relevance to understanding realistic core collapse believed to occur in nature. Current spherical calculations indicate that, of the proposed mechanisms for rapid, supernova envelope ejection following the collapse of a 1.4 $M_\odot$ core—i.e., momentum or energy deposition by

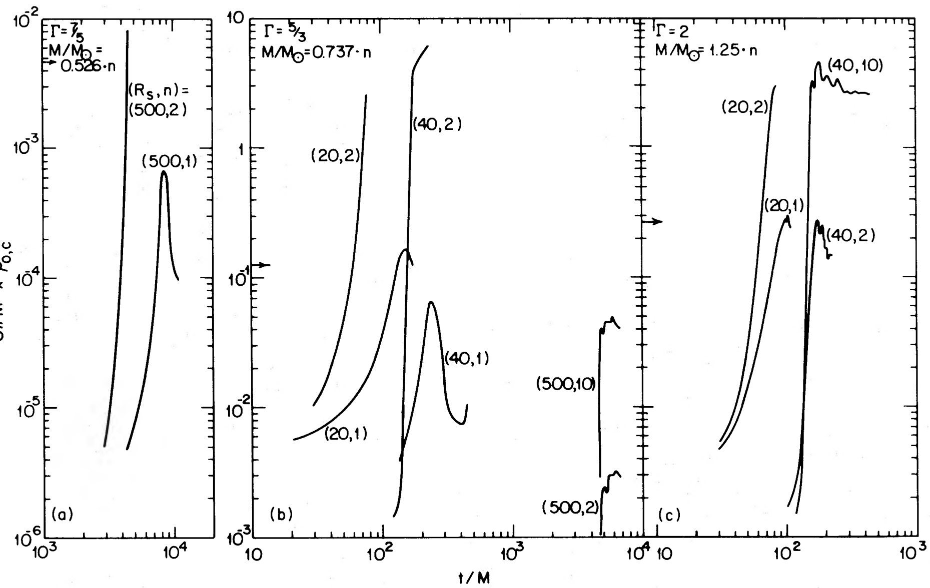

FIG. 5.—Time evolution of the central rest mass densities for the canonical collapse sequence summarized in Table 2. The quantities in parentheses denote, respectively, the initial Schwarzschild core radius and the multiple of M_A, M_B, or M_C adopted for the core mass. Arrows on the vertical axes denote the central densities for M_A, M_B, and M_C in (*c*), (*b*), and (*a*), respectively.

neutrinos, or a strong, reflection shock following a homologous core bounce (see, e.g., Bruenn, Arnett, and Schramm 1977 for a discussion and references)—the reflection shock scenario appears to be the most promising. Recent hydrodynamical calculations with realistic equations of state and neutrino transport (Arnett 1977; Wilson 1979*a*, *b*) indicate that neutrino transfer is strongly inhibited by the large, neutral-current core opacity. As a result, neutrino luminosities ($L_\nu \lesssim 8 \times 10^{52}$ ergs s^{-1}) remain well below the critical Eddington value, $L_{\rm Edd} \sim 10^{54}$ ergs s^{-1}, required for mass ejection by neutrino momentum transfer alone. However, neutrino trapping keeps the core adiabatic (with $\Gamma \lesssim 4/3$) and the lepton number high during the collapse, so that the pressure deficiency and flow Mach number never become large. Accordingly, the inner core experiences a *homologous* bounce at nuclear density (where Γ stiffens above 4/3) and drives a strong, reflection shock into the mantle and envelope. Although the ability of the shock to eject these other layers appears to depend sensitively on the model parameters, very recent spherical calculations by Wilson (1979*b*) indicate that ejection does indeed occur.

Recent ellipsoidal calculations of nonspherical, collapsing 1.4 $M_\odot$ cores with rotation indicate that the eccentricity of the inner core, though small initially, can grow dramatically if the core experiences a few large-amplitude, homologous oscillations following maximum compression (Saenz and Shapiro 1979). The eccentricity growth can result in a significant, time-varying quadrupole moment which leads to the efficient generation of gravitational radiation ($\Delta E_{\rm GR}/Mc^2 \sim 10^{-4}$–$10^{-2}$). Surprisingly, this behavior is found even for slowly rotating configurations with $J \gtrsim 5 \times 10^{46}$ erg-s and may thus apply to "canonical" collapse cases leading to neutron stars (e.g., the Crab pulsar). Moreover, the growth of the initially small nonspherical distortion during the collapse may trigger several new processes—e.g., large-scale convection which may force the trapped neutrinos to the core surface, where they can rapidly escape (Epstein 1979; Colgate 1978; Smarr, Taubes, and Wilson 1979)—that can assist in the ejection of the envelope on dynamical time scales.

Evidently, *mass ejection and gravitational wave generation during core collapse may depend crucially on the presence of homologous bounce behavior* following the initial infall. Homologous bounces can occur if pressure (entropy) deficiencies do not become large during the collapse and if Γ exceeds 4/3 eventually to induce the bounce. Such a scenario results from the high-temperature, adiabatic equation of state of Lamb *et al.* (1978) (see also Bethe *et al.* 1979) in which Γ remains slightly less than 4/3 until nuclear densities are achieved, when Γ stiffens to, e.g., $\Gamma \sim 2.5$. The (constant)$\Gamma = 7/5$ numerical calculations described in the previous section, where collapse is induced by a small pressure deficiency but results in a bounce (for $M < M_{\rm max}$) since $\Gamma > 4/3$, provides a qualitative picture of the behavior expected from such an equation of state.

Any significant departure from the above scenario (e.g., rapid entropy dissipation by some new, temperature-sensitive, central neutrino source) can lead to *nonhomologous* bounce behavior. Such an outcome will not result in mass ejection via core bounce or significant gravitational radiation, but will generate sufficient entropy following maximum compression to temporarily support the configuration against further collapse until neutrinos dissipate the thermal energy ($\Delta t_\nu \gtrsim 10$ s). We can only speculate in this case on the existence of a gradual energy pumping mechanism which could operate on a *dissipative* time scale to slowly detach the outer layers of the star, and prevent catastrophic collapse (cf. Domoyatskii and Nadezhin 1978). The magnetic-dipole luminosity of a central pulsar, proposed to explain Type II events, may furnish one such mechanism (Ostriker and Gunn 1971; Bodenheimer and Ostriker 1974), but the characteristic acceleration time scale ($\Delta t_{\rm md} \gtrsim 10^6$ s) appears to be too long here.

It should further be emphasized that, while present work indicates a core mass of $\sim 1.4\ M_\odot$, convection could lead to core masses much larger than $M_{\rm max}$ (Arnett, private communication). The fate of such a massive core is an open question: conceivably, the collapse to a black hole could occur nonhomologously on dissipative time scales as well as directly.

b) *Accreting Neutron Stars*

Neutron stars with masses near, but slightly less than, the maximum mass, may undergo catastrophic collapse to black holes by the accretion of additional gas. Such an event may take place in an X-ray binary system, where gas is supplied to the neutron star by the normal primary, or during a supernova explosion when the unejected outer envelope falls back onto the relaxed core.

We have employed our computer code to analyze, in a preliminary fashion, accretion-driven core collapse. We consider two stable, equilibrium neutron stars, denoted by A' and C in Figure 1 and Table 1, which obey the $\Gamma = 2$ and $7/5$ equations of state, respectively, as defined above. At the surface of each star we place a homogeneous shell of gas which satisfies the same equation of state as the underlying star and is initially at rest. We treat two cases, in which the constant mass-energy density of the shell is chosen to give a total mass M less than and greater than $M_{\rm max}$. The Eulerian rest-density profiles at $t = 0$ are shown in Figure 6 for the four distinct cases analyzed. (The apparent variation in the underlying neutron star density profile results from the scaling with M.) The initial and final core parameters, and ultimate fates, are summarized in Table 3. The world lines of Lagrangian matter tracers in the neutron stars and overlying shells are plotted in Figure 7 for $\Gamma = 7/5$ and in Figure 8 for $\Gamma = 2$.

For both equations of state, the dumping of additional mass onto the surface of an equilibrium configuration leads to catastrophic collapse to a black hole if the total mass of the configuration exceeds $M_{\rm max}$ (Figs. 7*b*, 6*b*). If the total mass is less than $M_{\rm max}$, the outer layers of the star are initially compressed by the infalling material, but rebound stably and participate in damped, acoustic oscillations lasting many envelope collapse time scales (Figs. 7*a*, 8*a*). In this case, a standing shock wave forms near the surface to decelerate the infalling gas until the bulk of the material has been accreted. The shock then propagates outward into the sparse atmosphere, but

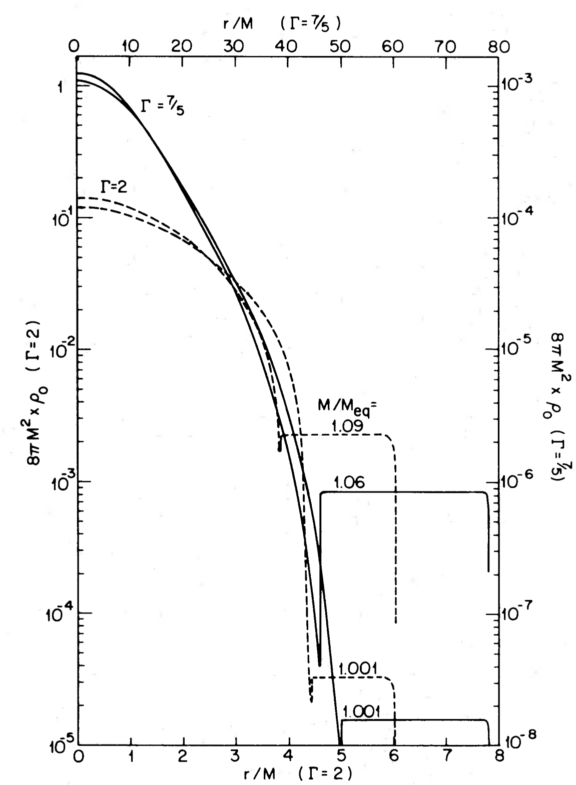

FIG. 6.—Initial Eulerian rest mass density profiles for the accreting neutron star models described in Table 3. Homogeneous shells at rest have been placed on stable, equilibrium neutron stars.

TABLE 3

PARAMETERS FOR THE ACCRETING NEUTRON STAR MODELS

		$t = 0$			$t = t_f$[a]				
Γ	M	R_s/M	$\rho_{0,c} \times 8\pi M^2$	α_c	t_f	$\rho_{0,c} \times 8\pi M^2$	α_c	$r_A(H)/M$	Outcome
2.......	$1.001M_{A'}$	7	0.12	0.577	54	0.45	0.27	...	oscillations
	$1.09M_{A'}$	7	1.14	0.566	72	1.37	3.4 (−9)	2.0	black hole
7/5.....	$1.01M_C$	80	1.1 (−3)	0.930	1.6 (3)	2.7 (−3)	0.91	...	oscillations
	$1.06M_C$	80	1.2 (−3)	0.929	1.0 (3)	5.1	4.3 (−13)	2.2	black hole

[a] $t = t_f$ is the time at the (arbitrary) termination of the numerical integrations.

forms again at the surface on successive oscillations. In the case of collapse, the infalling material drives a compression wave from the surface toward the stellar center; this wave initiates the collapse in successive radial shells as it steepens into a shock and propagates inward supersonically.

IV. THE GEOMETRY OF SPHERICAL COLLAPSE

A typical spacetime geometry for spherical collapse is shown in Figure 9, corresponding to the hydrodynamical scenario of Figure 2*b*. We probe the geometry by emitting outgoing radial light rays from various radii at various times. For example, a light ray emitted from the center of the star at $t = 170.0M$ gets out to infinity, while one

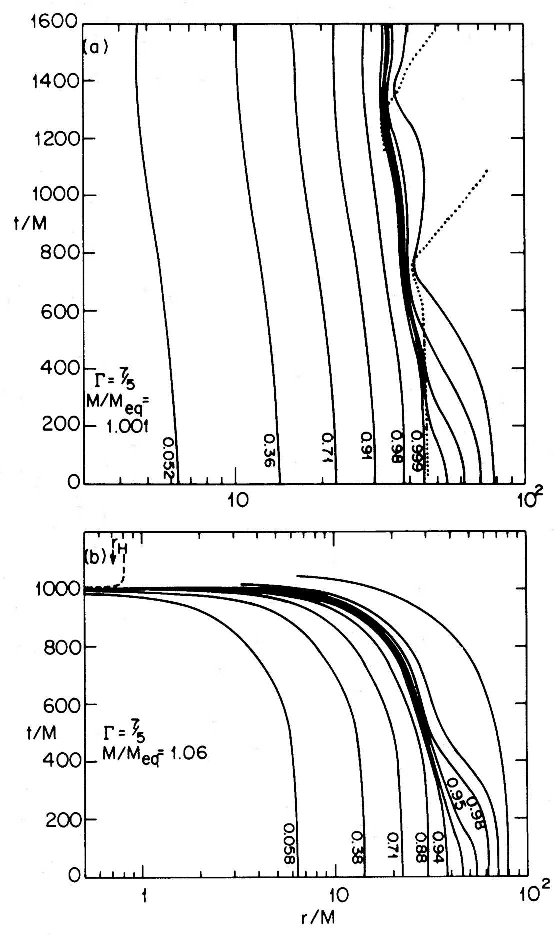

FIG. 7.—Spacetime diagrams for the world lines of Lagrangian matter tracers for the $\Gamma = 7/5$ accretion cases shown in Fig. 6. Each tracer is labeled by the fixed fraction of baryons interior to it. Dotted lines in (*a*) denote the shock fronts; the dashed line in (*b*) denotes the event horizon. The quantity r_H is the value of r at which $Ar = 2m$ (see § IV). If the total mass exceeds $M_{\max}$, a black hole forms.

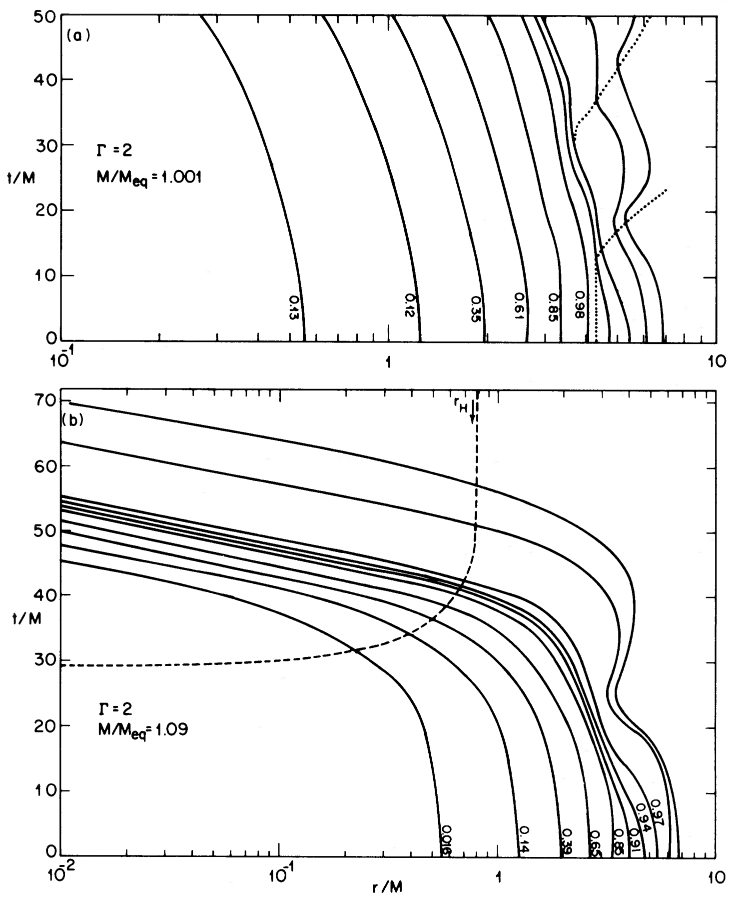

FIG. 8.—Spacetime diagrams for the world lines of Lagrangian matter tracers for the $\Gamma = 2$ accretion cases shown in Fig. 6. Labels are defined in the legend to Fig. 7.

emitted at $t = 170.9M$ does not. Thus the event horizon forms at the center between these times. By similarly finding pairs of light rays emitted from the same radius, one of which escapes and one of which does not, we can trace the growth of the event horizon as more and more matter flows into the black hole.

The shaded portion of the diagram represents the region of trapped surfaces, where even an outgoing spherical flash of light immediately becomes a sphere of smaller area. The apparent horizon (outermost trapped surface), always lies inside the event horizon, in accordance with theorems on black hole horizons (Hawking and Ellis 1973). The trapped region is actually bounded away from $r = 0$, but the nontrapped region is at exceedingly small values of the isotropic radial coordinate that we use. This is because of the development of a "throat" inside the black hole—a region where the circumferential radius, Ar, hardly changes while r decreases over many decades. Only when r is sufficiently small does Ar go to zero. This peculiarity of the radial coordinate is also responsible for the "turning up" of the light rays and matter world lines near $r = 0$ in Figure 9.

Because we solve elliptic equations for the metric functions, we are required to impose boundary conditions at the center of the star even when the center is inside the event horizon. As the throat grows with time, more and more of our radial grid is required to cover the throat, leaving less and less in the physically interesting region outside: the grid is "sucked down" the black hole. This is at present the factor limiting our ability to integrate indefinitely into the future outside the black hole. A similar grid sucking problem was encountered by Estabrook *et al.* (1973), who maximally sliced a vacuum Schwarzschild black hole. They used a zero shift vector β, and conjectured that a nonzero β would avoid grid sucking. Our work shows that this is not a general solution. We have also experimented with the grid velocity (cf. § II) in an attempt to counter the grid sucking, but without success. It remains a possibility that relaxing the maximal slicing condition (e.g., $\mathrm{Tr}\, K = \text{constant} \neq 0$; cf. Smarr and Eardley 1979) will alleviate the difficulty.

The size of a radial zone at the horizon at $t = 220M$ is shown at the top of Figure 9. The zone is a factor of 5 bigger than it was at the same radius when the horizon first formed. The event horizon, apparent horizon, and r_H all lie in the same radial zone, indicating reasonable accuracy in the solution. Here r_H is the value of r at which $Ar = 2M$.

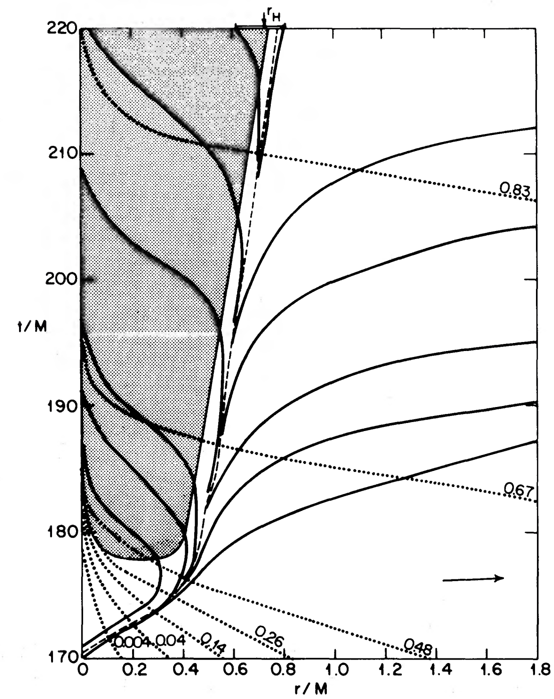

FIG. 9.—Spacetime geometry for the collapse case shown in Fig. 2*b*. Dotted lines are the world lines of Lagrangian matter tracers labeled by the fixed fraction of baryons interior to them. Solid lines denote outgoing radial light rays. The arrow shows the slope of a light ray at asymptotically large radii. The dashed line denotes the event horizon. The shaded area represents the region of trapped surfaces. The quantity r_H is the value of r at which $Ar = 2m$. The radial grid spacing near r_H at $t/M = 220$ is marked at the top of the diagram. Note that approximately one-half of the matter is still outside the black hole when a trapped surface first appears. Previous codes could not follow the evolution beyond this point owing to the formation of singularities (see text).

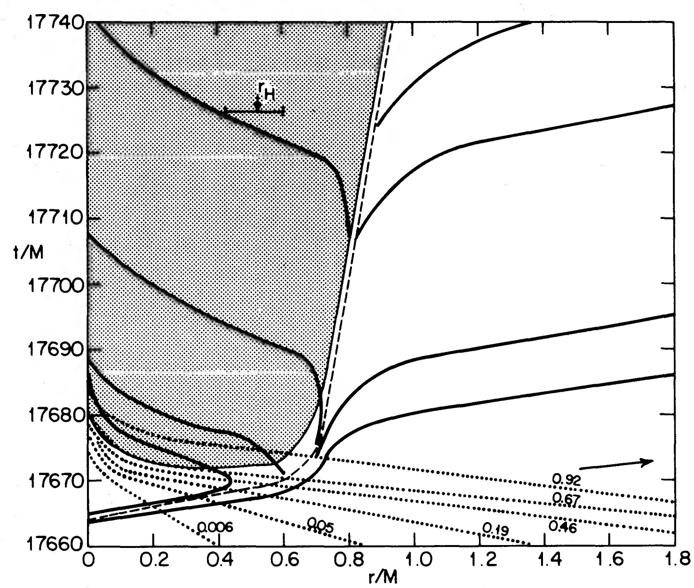

FIG. 10.—Spacetime geometry for the $\Gamma = 4/3$ collapse case described in Table 2. Labels are defined in the legend to Fig. 9.

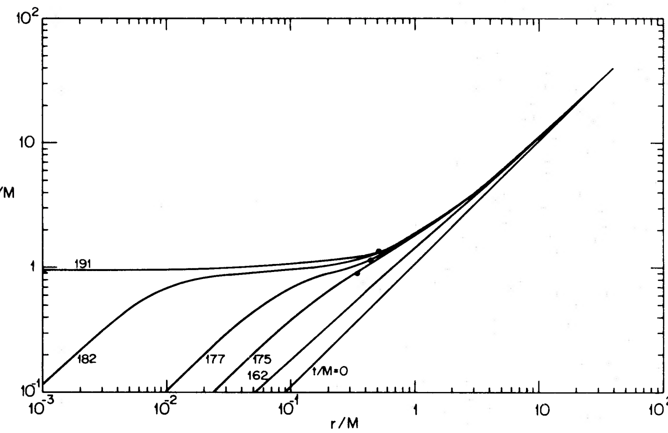

FIG. 11.—Circumferential radius Ar compared with isotropic radial coordinate r at different times for the case shown in Fig. 9. Dots denote the position of the event horizon. Note the growth of the "throat" at late times (see text).

Figure 10 is the analogous diagram for collapse of an initially homogeneous star from $500M$ with $\Gamma = 4/3$ and pressure reduced to half its equilibrium value. The geometry is qualitatively similar, when one allows for the longer time spend in Newtonian free fall. The accuracy implied by the position of r_H at the time shown is worse than in the previous case, because of the larger number of radial zones that is required (but was not employed) to follow collapse from a larger radius.

The growth of the throat is shown in Figure 11 for the $\Gamma = 5/3$ case illustrated in Figure 9. At later times, the region of r inside the black hole (to the left of the dots on each line) where Ar is constant gets larger and larger.

Values of the central lapse and scale factor as functions of time are shown in Figure 12 for the same case. The exponential "collapse of the lapse" (Smarr and York 1978*b*) is the result of maximal slicing attempting to hold back proper time at the center of the star to avoid the singularity in the future. For a coordinate-time step $\Delta t/M = 1$, a proper time of $\Delta\tau/M = 1$ elapses for an observer at infinity while only $\Delta\tau/M = 10^{-16}$ elapses for an observer at the center of star at the end of the integration. Corresponding to the decrease in α is a growth of A at $r = 0$. The apparent breaks in the curves for α_c and A_c at $t \sim 200M$ may not be real. Both α and A change smoothly to of order unity at large r.

One might try to avoid grid problems with the throat by using a Schwarzschild radial coordinate $r_s = Ar$. Unfortunately this leads to the development of a coordinate singularity when most of the matter is inside $r_s = 2M$. The choice of different radial coordinates can be thought of geometrically as different choices of the shift vector β. Smarr and York (1978*a*) have investigated the question of minimizing the "coordinate shear" by a suitable choice of β. Isotropic coordinates, as used in this paper, are the minimum shear coordinates for spherical spacetimes. Heuristically, one can say that isotropic coordinates remove the shear from the interior of the region between $r = 0$ and $r = \infty$, and place it all at the boundary point $r = 0$. Here A becomes very large, but varies smoothly enough to allow accurate numerical integration.

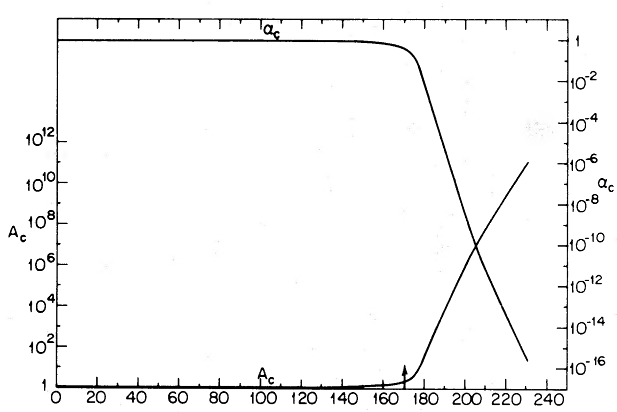

FIG. 12.—Time evolution of central values of the lapse α and the scale factor A for the case shown in Fig. 9. The arrow on the abscissa marks the time of formation of the event horizon at the center of the star.

Note that a May and White code goes singular in a time $\sim M$ after the formation of a trapped surface. In the case of Figure 9, this corresponds to $t \sim 179M$, when only 50% of the mass is inside the black hole.

V. DISCUSSION

The principal virtue of the numerical scheme presented here for handling gravitational collapse is evident: collapse to black holes can now be followed accurately on the computer so that the evolution outside can be determined far into the future without having the integration terminate because of spacetime singularities inside. The principal limitations of the current calculations are equally obvious: the collapse is assumed to be adiabatic and spherically symmetric. Dissipation and energy transport (e.g., via neutrinos), crucial to describing realistic core collapse, have not been incorporated as yet. The presence of finite angular momentum and initial asymmetries, which may fundamentally alter the core evolution and are imperative for the generation of gravitational radiation, have also been ignored.

Work is now in progress to remove the above local and global physical restrictions on the relativistic collapse code presented in this paper. Refinements in the adiabatic, spherical code are also underway, since this idealized case will presumably serve as a numerical and physical benchmark for future calculations. We hope to report progress in these areas in future papers.

It is a pleasure to thank Drs. Larry Smarr and Jim Wilson for useful discussions and for an unpublished version of their computer code for spherical collapse.

This work has been supported in part by the National Science Foundation grants AST 78-20708 and PHY 78-09795 at Cornell University.

REFERENCES

Arnett, W. D. 1977, *Ap. J.*, **218**, 815.
Arnowitt, R., Deser, S., and Misner, C. W. 1962, in *Gravitation*, ed. L. Witten (New York: Wiley) (ADM).
Bethe, H. A., Brown, G. E., Applegate, J., and Lattimer, J. M. 1979, preprint.
Bicknell, G. F., and Henriksen, R. N. 1979, *Ap. J.*, **232**, 670.
Bodenheimer, P., and Ostriker, J. P. 1974, *Ap. J.*, **191**, 465.
Bruenn, S. W., Arnett, W. D., and Schramm, D. N. 1977, *Ap. J.*, **213**, 213.
Colgate, S. A. 1978, Los Alamos preprint LA UR-78-2030.
Domoyatskii, G. V., and Nadezhin, D. K. 1978, *Soviet Astr.—AJ*, **22**, 297.
Epstein, R. E. 1979, *M.N.R.A.S.*, **188**, 305.
Estabrook, F., Wahlquist, H., Christensen, S., DeWitt, B., Smarr, L., and Tsiang, E. 1973, *Phys. Rev. D*, **7**, 2814.
Harrison, B. K., Thorne, K. S., Wakano, M., and Wheeler, J. A. 1965, *Gravitation Theory and Gravitational Collapse* (Chicago: University of Chicago Press).
Hawking, S. W., and Ellis, G. F. R. 1973, *Large Scale Structure of Space-time* (Cambridge: Cambridge University Press).
Lamb, D. Q., Lattimer, J. M., Pethick, C. J., and Ravenhall, D. G. 1978, *Phys. Rev. Letters*, **41**, 1623.
May, M., and White, R. H. 1966, *Phys. Rev.*, **141**, 1232.
———. 1967, *Meth. Comp. Phys.*, **73**, 219.
Misner, C. W., Thorne, K. S., and Wheeler, J. A. 1973, *Gravitation* (San Francisco: Freeman) (MTW).
Ostriker, J. P., and Gunn, J. E. 1971, *Ap. J. (Letters)*, **164**, L95.
Saenz, R. A., and Shapiro, S. L. 1979, *Ap. J.*, **229**, 1107.
Shapiro, S. L., Smarr, L., Teukolsky, S. A., and Wilson, J. R. 1980, in preparation (SSTW).
Smarr, L., and Eardley, D. M. 1979, *Phys. Rev. D*, **19**, 2239.
Smarr, L., Taubes, C., and Wilson, J. R. 1979, preprint.
Smarr, L., and York, J. W. 1978*a*, *Phys. Rev. D*, **17**, 1945.
———. 1978*b*, *Phys. Rev. D*, **17**, 2529.
Wilson, J. R. 1972, *Ap. J.*, **173**, 431.
———. 1979*a*, in *Sources of Gravitational Radiation*, ed. L. Smarr (Cambridge: Cambridge University Press).
———. 1979*b*, in *Proceedings of the Ninth Texas Symposium*, Munich, Germany, in press.
Van Riper, K. A. 1978, *Ap. J.*, **221**, 304.
———. 1979, *Ap. J.*, **232**, 558.
Van Riper, K. A., and Arnett, W. D. 1978, *Ap. J. (Letters)*, **225**, L129.

Stuart L. Shapiro and Saul A. Teukolsky: Center for Radiophysics and Space Research, Cornell University Ithaca, NY 14853